

Dispersion and Shear Modulus Measurements of Porcine Liver

MARKO ORESCANIN,^{1,3} MUQEEM A. QAYYUM,^{2,3} KATHLEEN S. TOOHEY^{2,3} AND
MICHAEL F. INSANA^{1,3}

¹*Department of Electrical and Computer Engineering*

²*Department of Bioengineering*

³*Beckman Institute for Advanced Science and Technology
University of Illinois at Urbana-Champaign
Urbana, IL 61801*

A narrow-band ultrasonic shear-wave imaging technique for estimating phase speed was applied to fresh and thermally damaged porcine liver *in vitro*. Two constitutive models were applied to the measurements to represent rheological behavior of the tissue and estimate the complex shear modulus at frequencies between 50 and 300 Hz. Our results were compared to similar values from the literature to assess how well models represent liver measurements over a range of shear-wave frequencies, experimental conditions and mammalian species. We found remarkable consistency in some parameters but not in others, suggesting that the Kelvin-Voigt model commonly applied in elasticity-imaging situations is representative of tissue dispersion but the description it offers is incomplete. Data are consistent with the theory that viscoelastic contrast is more likely due to changes in protein and other biomolecular-scale structures than from tissue anatomy larger than a cell. Dispersion measurements at frequencies between 0.5-1000 kHz are needed to more completely evaluate models for the viscoelastic behavior liver.

Key words: Constitutive models; thermal liver damage; viscoelasticity.

I. INTRODUCTION

Rheological models of organ and tissue material properties are playing significant roles in developing image-guided medical diagnoses and surgical procedures. During the previous two decades, advances in instrumentation and modeling have led to improvements in elasticity imaging and its interpretation for discriminating benign from malignant breast lesions,^{1,2} staging liver fibrosis,^{3,4} monitoring tumor ablation,⁵ assessing myocardial function,^{6,7} screening for prostate cancer⁸ and probing neurodegenerative processes in the human brain.⁹ The diagnostic information provided by elasticity imaging originates with the important role of the *microscopic* cellular mechanoenvironment in establishing homeostasis and regulating disease progression.^{10,11} It is thought that these microscopic effects influence the appearance of tissues in elasticity images by modifying *macroscopic* tissue structures. Rheological modeling aims to summarize the material properties of complex-structured media by representing it as a simple mechanical system characterized by just a few parameters. When the mechanical response of the model system closely represents tissue measurements, we assign model parameters to represent tissue properties at the spatiotemporal scale of the measurement. The value of elasticity imaging depends, in part, on how well model parameters represent tissue behavior.

2660161-7346/10 \$18.00

Copyright 2010 by Dynamedia, Inc.

All rights of reproduction in any form reserved.

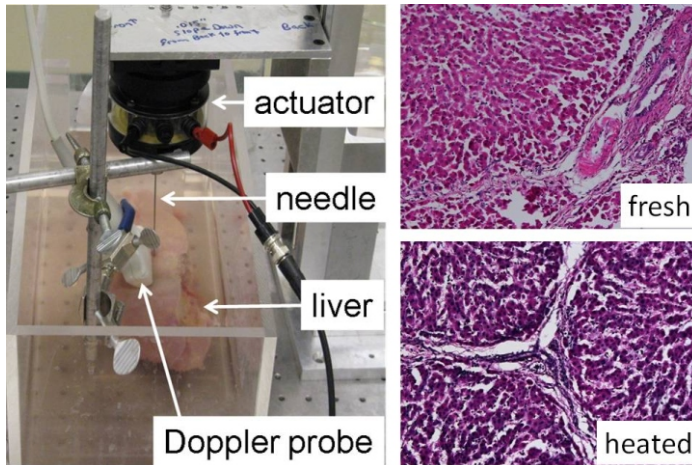


FIG. 1 (Left) Photograph of a shear-wave imaging experiment using fresh porcine liver. (Right) Histological sections of fresh and thermally -damaged porcine liver samples at 20x magnification.

The principal aim of the study reported here is to observe how well standard rheological models represent measurements of shear-wave speed in parenchymal tissues. We estimated the complex modulus of fresh, *ex vivo* porcine liver because the modulus can be modified by heating the tissue, measurements could be readily verified through literature comparisons and the results contribute to the accumulating data on assessments of thermal tissue damage induced during ablation procedures. We applied standard linear-solid two-parameter (Kelvin-Voigt or K-V) and three-parameter (Zener) rheological models.¹²

The basic measurement applies pulsed-Doppler techniques to image particle velocities associated with shear-waves radiating from a harmonically vibrating needle placed in the liver tissue sample.¹³ The phase speed of cylindrical shear-wave estimates \hat{c}_s is measured from the spatial-phase gradient. Speed estimates are numerically fit to modeled values to find the complex shear modulus. From \hat{c}_s and liver density ρ , the shear attenuation coefficient can be estimated.

II. METHODS

A. Tissue preparation

Six freshly-excised whole porcine livers were obtained in pairs during three different days from the Department of Animal Sciences at the University of Illinois. Mechanical studies were conducted on one fresh and one heated liver sample, as illustrated in figure 1. Each organ appeared to be healthy and free from obvious lesions or other structural anomalies. Livers were placed in iced saline (0.9% sodium chloride) immediately after harvesting and then transported to the lab for measurement. Once in the lab, fresh livers were warmed in normal saline at 23°C for one hour before mechanical testing.

Thermally-damaged livers were prepared by placing a fresh liver in saline heated to 47°C for 90 minutes. The aim was to thermally denature proteins¹⁵ and modify the collagen cross linking to alter the viscoelastic properties of the liver. After the heating period, livers were cooled in 23°C saline for one hour prior to mechanical testing. All liver measurements were made at 23°C within eight hours of harvesting.

Following each experiment, a small liver sample was prepared for histological study. Tissues were fixed with formalin, embedded in paraffin for sectioning and stained with

hematoxylin and eosin. Slides were examined by a pathologist for structural changes that might correlate with mechanical measurement observations. No significant histological changes were observed. Examples of fresh and thermal-damaged tissues can be seen in figure 1.

B. Shear-wave phase speed estimation

A 17-gauge stainless-steel needle (13-cm long) was inserted 3-5 cm into a liver sample (Fig. 1) and vibrated sinusoidally in time along its long axis by a mechanical actuator (SF-9324, PASCO Scientific, Roseville, CA). The actuator was driven by 500-ms-duration pure-tone voltage bursts (15 V) from a waveform generator at single frequencies in the range of 50 Hz to 300 Hz. In this range, the measured vibration amplitude was 10-250 μ m. Vibration generates harmonic shear waves that propagate radially from the needle for several millimeters before the mechanical energy is absorbed. Shear waves are tracked with a Doppler probe, where actuator motion and Doppler transmissions are electronically synchronized. Imaging the needle and adjacent tissues simultaneously, we found there was negligible needle slippage.

A Sonix-RP system (Ultrasonix Medical Corp, Richmond, BC, Canada) was used to estimate particle velocity as shear waves passed through the liver. A BW-14/60 linear-array transducer was driven by 6-cycle Doppler pulses at a center frequency of 6.67 MHz and a Doppler angle of $35 \pm 5^\circ$. The peak echo frequency was found to be ~ 6 MHz. We used the default beamformer for the array resulting in 128 A-lines separated laterally by a 0.46-mm array pitch. We acquired a 3000-pulse ensemble of echoes at each of the 128 lateral spatial locations at a pulse repetition frequency of 10 kHz. Echoes were sampled in fast time at 40 Msamples/s and then downsampled internally by a factor of two before data were transferred for off-line processing on a PC. We summarize the estimation of shear-wave speed from Doppler echoes below; however, readers are referred to reference 13 for details.

The first 500-1,000 Doppler traces are discarded to eliminate the shear-wave transient as the needle begins to vibrate. Particle velocity is then estimated from an ensemble grouping of 6 sequential echo traces in slow-time t_s using autocorrelation techniques.¹⁶ This process yields ~ 400 temporal velocity estimates at each radial location r and range time t . Note that in the shear-wave image shown below, the lateral dimension is r and the axial dimension is $z = ct/2$, where c is the compressional-wave speed. Shear speed c_s is estimated from the spatial wave phase as we now explain.

Let $\hat{v}[l, n, m]$ be the discrete form of the complex analytic signal for particle velocity, where l, n, m are integers. Here $r = lX$, $t = nT$ and $t_s = mT_s$ for sampling intervals in radial position, fast and slow times, $X = 0.46$ mm, $T = 25$ ns and $T_s = 0.1$ ms, respectively. We further average 40 velocity estimate along slow time (after the transient wave has dissipated) and compute a four-sample running mean in radial position to form the shear-wave spatial-phase estimate,

$$\hat{v}_s(l, n) = \frac{1}{40} \sum_{m=1}^{40} \frac{1}{3} \sum_{l=1}^3 \hat{v}^*(l, n, m) \hat{v}(l+1, n, m) \quad (1)$$

At angular shear-wave frequency ω and tissue location $(r, z) = (lX, cnT/2)$, the shear-wave phase speed estimate is

$$\hat{c}_s(\omega, r, z) = \frac{X}{\arg[\hat{v}_s(l, n)]} \quad (2)$$

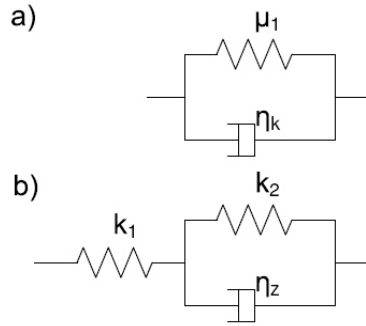


FIG. 2 Parametric representations of the standard linear-solid two-parameter (Kelvin-Voigt) and three-parameter (Zener) rheological models. μ_1 is the elasticity shear constant, η_{kz} is the dynamic viscosity constant for the K-V or Zener models and $k_{1,2}$ is an elastic spring constant.

Equation (2) is a practical implementation of the phase gradient expression, $d^- / dr = c_s(\omega)$, which is derived in reference 13 and is based on the discussion in reference 17.

C. Complex modulus estimation

The complex shear modulus $\mu(\omega)$ is estimated from the shear speed dispersion curve, $c_s(\omega)$. The association between the two functions is through the complex shear wave number, $k_s(\omega) = \omega/c_s(\omega) + i \alpha_s(\omega) = (\omega^2/\mu(\omega))^{1/2}$, where $\alpha_s(\omega)$ is the shear-wave attenuation coefficient and ρ is mass density. Expressing k_s in terms of real $\{R\}$ and imaginary $\{I\}$ components, yields³⁶

$$c_s(\omega) = \omega / R\{k_s\} \sqrt{\frac{2 R\{k_s\}^2 - I\{k_s\}^2}{R\{k_s\} \sqrt{R\{k_s\}^2 + I\{k_s\}^2}}} \tag{3}$$

and

$$\alpha_s(\omega) = I\{k_s\} \sqrt{\frac{2 \sqrt{R\{k_s\}^2 + I\{k_s\}^2} R\{k_s\}}{2 R\{k_s\}^2 - I\{k_s\}^2}} \tag{4}$$

that require adoption of a rheological model to carry out the computations.

The Kelvin-Voigt model illustrated in figure 2a is frequently employed in imaging experiments where forces are applied to a viscoelastic material and strain is measured over time. The complex modulus for the Kelvin-Voigt model,

$$K(\omega) = \mu_1 + i \eta_k \omega \tag{5}$$

has one elastic and one viscous component in parallel. The elastic shear constant is μ_1 , which is also referred to as the relaxed modulus because $\lim_{\omega \rightarrow 0} K(\omega) = \mu_1$. The dynamic viscosity constant is η_k . Viscous dissipation of shear-wave energy is also quantified by the quality factor $Q(\omega) = \mu_1 / \eta_k \omega$, whose inverse¹⁹ is the dissipation factor Q^{-1} . For the Kelvin-Voigt model,

$$Q^{-1}(\omega) = \eta_k \omega / \mu_1 \tag{6}$$

where $\tau = \eta/\mu_I$ is a relaxation time constant. The frequency dependence of Q^{-1} shows that K-V dissipation is unbounded and increasing with frequency. Thus, the Kelvin-Voigt model describes the viscoelastic behavior of liver tissues as a low-pass filter of shear-wave energy.

The Zener model illustrated in figure 2b adds an elastic element in series with the K-V unit to allow for more complex dynamic behavior.¹⁹ It has been shown to accurately represent the viscoelastic behavior of human liver *in vivo* in the shear frequency range of 25 to 62.5 Hz.²⁰ The complex modulus obtained from the Zener model is

$$z(\omega) = \frac{1}{1 + \tau^2 \omega^2} + i \frac{\tau \omega}{1 + \tau^2 \omega^2} \quad (7)$$

where $\mu_1 = \frac{k_1 k_2}{k_1 + k_2}$ is the relaxed modulus and $\tau = \eta/(k_1 + k_2)$ and $\tau = \eta/k_2$ are associated relaxation times. For the Zener model,

$$Q = \frac{1}{1 + \tau^2 \omega^2} \quad (8)$$

Systems represented by the Zener model exhibit purely elastic behavior at both ends of frequency spectrum where $Q^{-1} \rightarrow 0$. Moreover, there exists a relaxation peak at $\omega = 1/\sqrt{\tau^2}$ and viscous losses are greatest. Thus, the Zener model describes the viscoelastic behavior of liver tissue as a band-stop filter of shear wave energy.

D. Rheometer testing

Liver samples were cut into cylindrical slabs to measure the shear stress relaxation using a controlled shear-strain rheometer (TA Instruments, Model AR-G2, New Castle, DE, USA). The rheometer had parallel circular plate fixtures, each 25 mm in diameter. Liver samples were first cut into slabs approximately 5 mm thick and then cut into cylinders 25 mm in diameter using a circular punch. To avoid having samples slip when torqued, water-proof sandpaper was fixed to the upper and lower rheometer plate surfaces. A small compressive load (<0.1 N) was applied to samples to ensure contact with the sandpaper and minimize slippage. A 5 percent rotational strain was applied to each sample for a period of 30 minutes with a one-second ramp-on time to study shear relaxation. Time-varying torque measurements were analyzed to estimate relaxation moduli through a 3rd-order generalized Maxwell model as previously described.²¹ No preconditioning was applied to liver samples.

E. Liver density

The mass density of liver samples was estimated in an independent measurement by applying Archimedes Principle. Liver samples free from major blood vessels were cut into roughly 10 g cubes and submerged into a beaker with 400 g of distilled water at 23 °C. Samples immediately sank to the bottom. Sodium chloride (Sigma Aldrich Inc., St. Louis MO) was added in 0.5 g increments and dissolved until the sample began to float. Then sodium chloride was added in 0.05 g increments until the liver became neutrally buoyant. Assuming the density of water is 1.00 g/cm³ and the density of sodium chloride is 2.16 g/cm³, we computed the density for three fresh and three thermally-damaged samples. Results are summarized in table 1. Our measurement values agree with others from the literature, where the density of porcine liver was reported to be 1.064 g/cm³ at 37 °C.²³ Our intention was not to characterize samples based on density, but to demonstrate that there is not a measurable difference between densities that could bias modulus estimates.

Table 1. Measured density of fresh and thermally-damaged porcine liver at 23 °C.

Fresh tissue (g/cm ³)	TD tissue (g/cm ³)
1.05	1.06
1.07	1.05
1.05	1.05
1.06 ± 0.01	1.06 ± 0.004

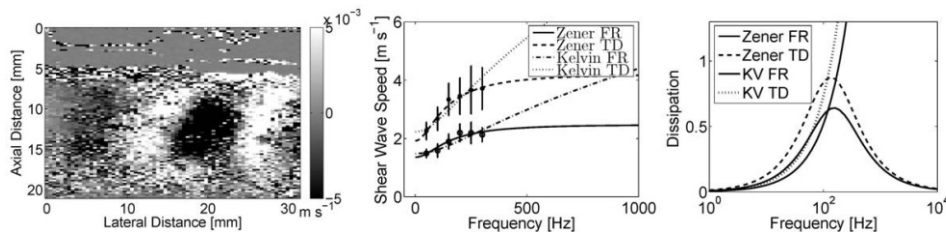


FIG. 3 (Left) Particle velocity image of a 100 Hz shear wave in fresh porcine liver tissue from one rf frame. Waves are generated by a needle vibrating near the dark elliptical center. The top surface of the sample is located at a depth of 5 mm. Comparison of shear wave speeds (middle) and dissipation factors (right) as a function of frequency for the Kelvin-Voigt and Zener models for both fresh (FR) and thermally-damaged (TD) porcine liver. Measurements are indicated by points that specify the mean \pm 1 SD.

III. RESULTS

Shear speed measurements between 50 and 300 Hz in steps of 50 Hz are computed for each of the three fresh and three thermally damaged liver samples. Values plotted in figure 3 (middle) are the average of the three samples at a given frequency. The Kelvin-Voigt and Zener models were numerically fit to the measured data using methods described previously.¹³ Lines plotted in the figure result from the parameters that gave the least-squares fit of model functions to speed measurements. Table 2 lists those parameters along with μ_1 estimates obtained from rheometer stress-relaxation measurements on samples from the same livers. Applying K-V model parameters to Eq. (4), we found at 100 Hz that $\nu_s = 0.94 \text{ cm}^{-1}$ for fresh liver and $\nu_s = 0.79 \text{ cm}^{-1}$ for thermally damaged liver.

We conducted a two-sample, unpaired, two-tailed Student's *t*-test of the null hypothesis that heating does not alter the shear speed of liver. Hypothesis testing was conducted at each frequency in figure 3 where shear speeds were estimated. The untested assumption is that tissue samples from the fresh and thermally-damaged classes of liver are normally distributed with equal variance. There were three measurement samples from each liver class, and we estimated class means from those samples. Therefore there are four degrees of freedom. We found for speed estimates at the six frequencies that the corresponding *p* values fell in the range of 0.0145 $\leq p \leq$ 0.0458. Therefore, we must reject the null hypothesis at the significance level of 0.05 and conclude, within the limits of the assumptions, that shear speed measurements of fresh and thermally damaged liver are distinct.

There is a small difference between dispersion curve models seen in figure 3 (middle). Consequently, either rheological model may be used to represent measured shear speeds within measurement error. From the model parameters of table 2, we generated mechanical dissipation curves Q^{-1} for the two models via Eqs. (6) and (8) and plotted them in figure 3

TABLE 2 Estimated viscoelastic parameters.

Rheological model	Porcine liver	[kPa]	[Pa s]			
Kelvin-Voigt model	fresh	2.2	1.8			
Kelvin-Voigt model	thermally damaged	5.0	5.8			
Zener model	fresh	1.8	k_1 [kPa]	k_2 [kPa]	ζ [Pa s]	
Zener model	thermally damaged	3.7	6.2	2.6	4.99	
Rheometer, 2% strain	fresh	0.06 ± 0.03	18	4.6	12	
Rheometer, 5% Strain	fresh	0.09 ± 0.02				
Rheometer, 2% strain	thermally damaged	0.14 ± 0.01				

(right). While the K-V model predicts a monotonic increase in wave energy loss with shear-wave frequency, the Zener model exhibits a dissipation resonance peak at $\omega/2 = 153$ Hz for fresh tissue and $\omega/2 = 135$ Hz for thermally-damaged liver tissue. Above $\omega/2$, the two models clearly diverge. Unfortunately, we were unable to obtain reliable shear speed estimates above 300 Hz in liver. We discuss the possible implications of this observation in the next section.

IV. DISCUSSION

The complex modulus was estimated from shear wave images obtained in large tissue samples that included at least one entire liver lobe. Reflected waves at tissue boundaries were negligible because of high shear-wave attenuation. We considered that nonphysiological conditions, such as the lack of liver perfusion and room temperature measurements, could affect the results as compared with *in vivo* findings. Others¹⁸ found that nonperfused porcine livers were stiffer and more viscous under cyclic compressive loads and the effects were found to be more pronounced when large preloads were applied to the liver. The shear-displacement amplitudes in our study produced strains $<1\%$ and there was no preload. Consequently, liver perfusion and temperature were not expected to be a major influence on viscoelastic properties, provided there was little degradation of the protein structure.

We attempted to validate our shear-wave measurements of the elastic shear constant μ_1 through comparisons with independent rheometer measurements of μ_1 . We found reasonably close agreement between rheometer and shear-wave estimates for gelatin in a previous study,¹³ however, table 2 shows that no such agreement for liver tissue was found. Estimates of μ_1 derived from the two techniques can be expected to agree for linear viscoelastic media, as we found gelatin to be, but liver parenchyma is known to deform nonlinearly. Indeed, Liu and Bilston²² found that shear relaxation moduli measured for bovine liver demonstrated significant strain and strain-rate sensitivities above 0.2% strains. Lacking an independent standard measurement, we decided to compare our measurements with those published by other labs.

In figure 4 (left), our measurements from figure 3 may be compared to those of Chen et al²⁸ who applied a shear-wave dispersion ultrasound vibrometry (SDUV) method to *in vivo* porcine liver. The principal experimental differences are the use of radiation force and their

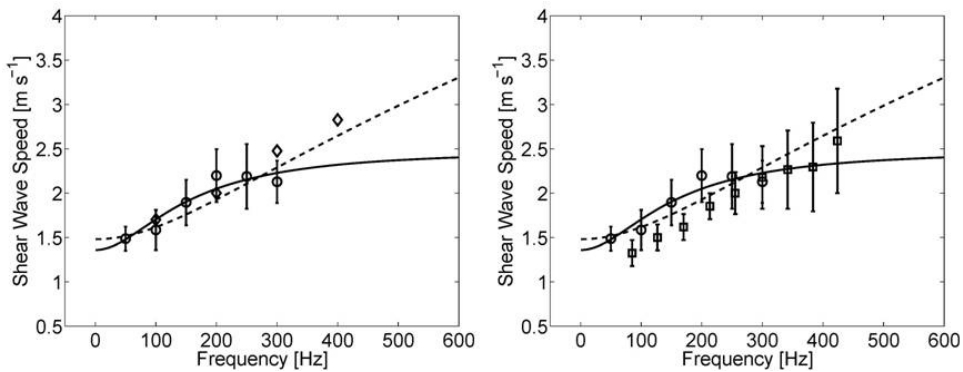


FIG. 4 Shear wave speed measurements in fresh *ex vivo* porcine liver from figure 3 are compared with two other measurement sets reported in the literature. Our measurements (circle-labeled points with error bars in both plots) and best-fit model curves are compared with the measurements of (left) Chen et al.²⁸, Fig. 6d), as indicated by diamond-labeled points, and (right) Deffieux et al.³⁴, Fig. 11, second volunteer), as indicated by square-labeled point with error bars. The K-V model values are indicated by the dashed curve and the Zener model values are indicated by the solid curve.

measurements were for perfused liver measured near normal body temperature. These authors measured speed from the spatial phase shift over a distance of 3-5 mm in liver and they assumed the K-V model when relating dispersion to modulus constants. There is close agreement between shear-speed estimates for the two labs up to 300 Hz. It is not surprising then that the complex modulus constants from the two labs are similar for porcine liver: 2.2 kPa, 1.8 Pa s (UIUC) and 2.4 kPa, 2.1 Pa s (Mayo). The agreement suggests that liver perfusion, temperature and measurement technique are not major factors in shear-wave measurements of μ_1 .

In figure 4 (right), our same measurements may also be compared to those of Deffieux et al.³⁴ They developed a supersonic shear-imaging technique (SSI) for *in vivo* shear wave spectroscopy (SWS) and adopted the K-V model to relate shear speed to modulus constants. Their *in vivo* measurements on healthy livers of human volunteers yielded speed estimates that are statistically comparable to ours, made on excised porcine liver. Shear-speed values appear to be slightly lower for human data relative to pig, which is consistent with the slightly lower value of μ_1 reported by Chen et al for humans via MRE methods relative to pigs. Although the findings are consistent and perhaps expected given known differences in lobular collagen content between humans and pigs, none of the observed species-specific differences in shear properties can be considered statistically significant when measurement uncertainties are considered.

Conversely, heating increased the stiffness and viscosity of *ex vivo* liver tissue, as detected by the significant increase in shear wave speed observed (Fig. 3). Assuming the heating regimen that we adopted¹⁵ produces protein denaturation and coagulative necrosis similar to that found following *in vivo* liver ablation procedures,³⁵ then it seems that thermally-induced biochemical changes to liver tissue influence the complex modulus to a greater extent than variations in anatomical structure. For example, the histology displayed in figure 1 showed no apparent thermally-induced changes in cellular architecture. We estimate a doubling of μ_1 in thermally-damaged liver compared to fresh liver. Others found as much as a four-fold increase in μ_1 that varied systematically with heating time and rate.²⁴ Previous results formed the basis for more recent studies exploring the use of elasticity imaging methods to track the growth of thermal lesions during ablation procedures.²⁵⁻²⁷ Our contribution to these results is

the findings of table 2 that the dynamic viscosity constant increases threefold after thermal damage as compared to a doubling of μ_1 . Thus μ_1 could be a more robust parameter for viscoelasticity imaging of thermal lesion growth in the 50-300 Hz bandwidth provided its measurement uncertainty is comparable to that observed for μ_1 .

Our technique does not provide enough measurement bandwidth to conclude whether one rheological model is more representative of liver dispersion. It is possible that our inability to easily sense shear-wave energy in liver above 300 Hz could be an indication that dissipation increases with frequency, as occurs directly with the K-V model. Fitting the first-order Zener model to liver dispersion measurements predicts a dissipation resonance at $\omega > \omega_0$ 150 Hz, and the nonintuitive result that attenuation should decrease with frequency. Adding more Kelvin-Voigt units in series with the first-order Zener model (Fig. 2b), each having increasing resonance frequency, would provide more degrees of freedom for modeling. Yet our confidence in modeling results degrades as the number of fit parameters increases without also increasing data samples. It is also true that as shear-wave frequency increases, the amplitude of the mechanical actuator is reduced¹³ and the potential for the needle slipping against the tissue is greater.

Determining the lowest-order constitutive model that best represents dispersion data up to about 1 kHz could provide new insights into the sources of viscoelastic tissue contrast created through disease processes or applied therapeutics. Model parameters conveniently summarize macroscopic rheological behavior of tissues, which offers us intuition regarding the relative degrees of elastic and dissipative responses that we often relate to constituent tissue components. What are the components of tissue that interact with shear wave energy? We believe that by extending the measurement bandwidth some of the answers are emerging. Specifically, consider the work of Frizzell and Carstensen³⁶ and Madsen et al¹⁴ who made measurements at 2-14 MHz, a frequency band five-orders of magnitude high. At shear-wave frequencies below 500 Hz, the wavelength is on the order of centimeters. At 8 MHz, the wavelength is just 6 μm . One might expect modulus values to vary significantly between these bandwidths if tissue structures larger than cells were responsible for the interaction. In the 50-300 Hz range for porcine and human liver, we measured shear speeds between 1-3 m/s and shear attenuation coefficients less than 2 cm^{-1} . At frequencies between 2-14 MHz, Frizzell and Carstensen and Madsen et al each independently measured shear-wave speeds at room temperature for bovine, rodent and canine liver samples in the range of 10-60 m/s and shear attenuation coefficients in excess of 10^4 cm^{-1} . Yet they found, assuming a K-V model, that $\mu_1 = 2.3 \text{ kPa}$ for bovine liver in the MHz range. This value is in line with measurements made at much lower frequencies, e.g., those in table 2I. They also found $\tau = 0.013 \text{ Pa s}$, lower by two orders of magnitude in the MHz frequency range as compared to the Hz range. (Note that τ is weighted by frequency in the expression for shear attenuation coefficient.) The apparent frequency dependence of τ is evidence that the K-V model is incomplete.

A similar conclusion was reached by others independently. It was found that a power-law relationship describing shear attenuation, which is based on the Kelvin-Voigt model, was unable to represent the fractional power-law relationship observed in soft biological tissue.³⁷ Szabo and Wu³⁸ reached the same conclusion during their study of polymer materials. They proposed a theoretical framework based on the K-V model that expands the dynamic viscosity component with fractional-derivative-like terms, effectively making a frequency dependant τ for the K-V model. This modification implies that classical models with combinations of springs and dashpots cannot model the shear modulus over the measurable frequency range. However, below 300 Hz, we and others found that the modulus is sensitive to thermal history, and yet parametric models respond similarly. So it is unnecessary to choose one model over another.

Conversely, the elastic shear constant μ_1 measured in the frequency range of 50-300 Hz is comparable to values measured in the MHz range, which suggests that μ_1 could be frequency independent as predicted by the K-V model. Shear measurements between 500 Hz and 1 MHz are needed to verify frequency independence. μ_1 appears to be invariant for liver among the mammalian species examined. While there are obvious macrostructural differences among the livers of various species, the cellular biochemistry and structure are very similar as are μ_1 estimates. Heating tissues, however, increases the average stiffness as it induces cellular necrosis and collagen fiber cross linking. Thus shear-wave energy interacts primarily with protein and other molecular-scale structures that are common among species but can change with disease. Absorption of shear-wave energy in liver is much stronger than scattering at all frequencies, apparently even more so than it is for compressional waves.³⁹⁻⁴¹

V. CONCLUSIONS

The Kelvin-Voigt rheological model predicts an elastic shear constant $\mu_1 \sim 2$ kPa for liver tissue over two distinct bandwidths of shear-wave frequencies: 50-300 Hz and 2-14 MHz. The elastic shear constant is invariant with mammalian species and degree of perfusion. Yet μ_1 is a sensitive indicator of thermal damage, a process known to modify tissue macromolecules. The dynamic viscosity 'constant' for liver tissue was found to vary significantly between the same two measurement bandwidths, and yet, it exhibits greater sensitivity than μ_1 to thermal damage. Taken together, the data suggest the K-V model may be an incomplete model but is adequate for assessing thermal effects below 300 Hz. Dispersion measurements made at shear-wave frequencies between 0.5 and 1000 kHz are needed to define the most appropriate and concise rheological model for representing viscoelastic behavior of liver.

Shear waves interact with mammalian tissue predominantly at the molecular scale through absorption. Consequently, elasticity imaging contrast from disease-induced changes can be expected to occur at a subcellular scale and is not greatly affected by tissue structures larger than a cell. Macromolecular changes that increase the complex modulus in heated liver could have counterparts in disease formation and therapeutic responses that also provide contrast. We need to more closely consider the role of molecular processes in elasticity contrast and to more completely probe the shear-wave frequency landscape to find constitutive models that concisely represent tissues.

ACKNOWLEDGMENTS

The authors gratefully acknowledge the Meat Science Laboratory in the Department of Animal Sciences at the University of Illinois for providing porcine liver tissues for this research, the Autonomic Materials Laboratory at the UIUC Beckman Institute for use of a rheometer and the Bioacoustics Research Laboratory at the Beckman Institute for use of their facilities. We also acknowledge the financial support of Dr. Lianjie Huang and the U.S. Department of Energy through the LANL/LDRD Program and the National Cancer Institute under award number R01 CA082497.

REFERENCES

1. Itoh A, Ueno E, Tohno E, et al. Breast disease: Clinical application of US elastography for diagnosis, *Radiology* 239, 341-350 (2006).

2. Qiu Y, Sridhar M, Tsou JK, et al. Ultrasonic viscoelasticity imaging of nonpalpable breast tumors: preliminary results, *Acad Radiol* 15, 1526-1533 (2008).
3. Castera L, Vergniol J, Foucher J, et al. Prospective comparison of transient elastography, fibrotest, APRI, and liver biopsy for the assessment of fibrosis in chronic hepatitis C, *Gastroenterology* 128, 343-350 (2005).
4. Huwart L, Sempoux C, Salameh N, et al. Liver fibrosis: Noninvasive assessment with MR elastography versus aspartate aminotransferase-to-platelet ratio index, *Radiology* 245, 458-466 (2007).
5. Fahey BJ, Nelson RC, Hsu SJ, et al. In vivo guidance and assessment of liver radio-frequency ablation with acoustic radiation force elastography, *Ultrasound Med Biol* 34, 1590-1603 (2008).
6. Kanai H. Propagation of spontaneously actuated pulsive vibration in human heart wall and in vivo viscoelasticity estimation, *IEEE Trans Ultrason Ferroelectr Freq Control* 52, 1931-1942 (2005).
7. Sack I, Rump J, Elgeti T, et al. MR elastography of the human heart: noninvasive assessment of myocardial elasticity changes by shear wave amplitude variations. *Mag Reson Med* 61, 668-677 (2009).
8. Weiss R, Egorov V, Ayrapetyan S, et al. Prostate mechanical imaging: A new method for prostate assessment. *Urology* 71, 425-429 (2008).
9. Sack I, Beierbach B, Wuerfel J, et al. The impact of aging and gender on brain viscoelasticity. *Neuroimage* 46, 652-657 (2009).
10. Discher DE, Janmey P, Wang YL. Tissue cells feel and respond to the stiffness of their substrate. *Science* 310, 1139-1143 (2005).
11. Butcher DT, Alliston T, Weaver VM. A tense situation: forcing tumour progression. *Nat Rev Cancer* 9, 108-122 (2009).
12. Tschoegl NW, *The Phenomenological Theory of Linear Viscoelastic Behavior: An Introduction*, (Springer-Verlag, Heidelberg, 1989).
13. Orescanin M, Insana MF. Shear modulus estimation with vibrating needle stimulation, *IEEE Trans Ultrason Ferro Freq Control* 57, 1358-1367 (2010).
14. Madsen EL, Sathoff HJ, Zagzebski JA. Ultrasonic shear wave properties of soft tissues and tissuelike materials, *J Acoust Soc Am* 74, 1346-1355 (1983).
15. Stylianopoulos T, Aksan A, Barocas V. A structural, kinetic model of soft tissue thermomechanics, *Biophys J* 94, 717-725 (2008).
16. Kasai C, Namekawa K, Koyano A, et al. Real-time two-dimensional blood flow imaging using an autocorrelation technique, *IEEE Trans Sonics Ultrason SU-32*, 458-463 (1985).
17. Hoyt K, Parker KJ, Rubens DJ. Real-time shear velocity imaging using sonoelastographic techniques, *Ultrasound Med Biol* 33, 1086-1097 (2007).
18. Kerdok AE, Ottensmeyer MP, Howe RD. Effects of perfusion on the viscoelastic characteristics of liver, *J Biomech* 39, 2221-2231 (2006).
19. Carcione JM. *Wave Fields in Real Media: Wave Propagation in Anisotropic, Anelastic and Porous Media*, (Elsevier Science Ltd., Oxford, 2001).
20. Asbach P, Klatt D, Hamhaber U, et al. Assessment of liver viscoelasticity using multifrequency MR elastography, *Mag Res Med* 60, 373- 379 (2008).
21. Orescanin M, Toohey K, Insana MF. Material properties from acoustic radiation force step response, *J Acoust Soc Am*, 125, 2928-2936 (2009).
22. Liu Z, Bilston LE. Large deformation shear properties of liver tissue, *Biorheology* 39, 735-742 (2002).
23. Ludwig GD. The velocity of sound through tissues and the acoustic impedance of tissues, *J Acoust Soc Am* 22, 862-866 (1950).
24. Kallel F, Stafford RJ, Price RE, et al. The feasibility of elastographic visualization of HIFU-induced thermal lesions in soft tissues, *Ultrasound Med Biol* 25, 641-647 (1999).
25. Lizzi FL, Muratore R, Deng CX, et al. Radiation-force technique to monitor lesions during ultrasonic therapy, *Ultrasound Med Biol* 29, 1593-1605 (2003).
26. Maleke C, Konofagou EE. Harmonic motion imaging for focused ultrasound (HMIFU): a fully integrated technique for sonication and monitoring of thermal ablation in tissues, *Phys Med Biol* 53, 1773-1793 (2008).
27. Kiss MZ, Daniels MJ, Varghese T. Investigation of temperature-dependent viscoelastic properties of thermal lesions in ex-vivo animal liver tissue, *J Biomech* 42, 959-966 (2009).
28. Chen S, Urban MW, Pislaru C, et al. Shearwave dispersion ultrasound vibrometry (SDUV) for measuring tissue elasticity and viscosity, *IEEE Trans Ultrason Ferroelectr Freq Control* 56, 55-62 (2009).

29. Fatemi M, Greenleaf JF. Ultrasound-stimulated vibro-acoustic spectrography, *Science* 280, 82-85 (1998).
30. Barannik EA, Girnyk A, Tovstiak V, et al. Doppler ultrasound detection of shear waves remotely induced in tissue phantoms and tissue in vitro, *Ultrasonics* 40, 849-852 (2002).
31. Konofagou EE, Hynynen K. Localized harmonic motion imaging: theory, simulations and experiments. *Ultrasound Med Biol* 29, 1405-1413 (2003).
32. Nightingale K, Soo MS, Nightingale R, et al. Acoustic radiation force impulse imaging: In vivo demonstration of clinical feasibility, *Ultrasound Med Biol* 28, 625-634 (2001).
33. Sinkus R, Siegmann K, Xydeas T, et al. MR elastography of breast lesions: understanding the solid/liquid duality can improve the specificity of contrast-enhanced MR mammography, *Magn Reson Med* 58, 1135-1144 (2007).
34. Deffieux T, Montaldo G, Tanter M, et al. Shear wave spectroscopy for in vivo quantification of human soft tissues visco-elasticity, *IEEE Trans Med Imaging* 28, 313-322 (2009).
35. Curley SA, Izzo F. Radiofrequency ablation of primary and metastatic hepatic malignancies. *Int J Clin Oncol* 7, 72-81 (2002).
36. Frizzell LA, Carstensen EL. Shear properties of mammalian tissues at low megahertz frequencies, *J Acoust Soc Am* 60, 1409-1411 (1976).
37. Sinkus R, Siegmann K, Xydeas T, et al. MR elastography of breast lesions: understanding the solid/liquid duality can improve the specificity of contrast-enhanced MR mammography, *Magnetic Resonance Med* 58, 1135-1144 (2007).
38. Szabo TL, Wu J. A model for longitudinal and shear wave propagation in viscoelastic media, *J Acoust Soc Am* 107, 2437-2446 (2000).
39. Goss SA, Frizzell LA, Dunn F, et al. Dependence of the ultrasonic properties of biological tissue on constituent proteins, *J Acoust Soc Am* 67, 1041-1044 (1980).
40. Parker KJ. Ultrasonic attenuation and absorption in liver tissue. *Ultrasound Med Biol* 9, 363-369 (1983).
41. Akashi N, Kushibiki J, Chubachi N, et al. Acoustic properties of selected bovine tissues in the frequency range 20-200 MHz, *J Acoust Soc Am* 98, 3035-3039 (1995).